Available online at www.sciencedirect.com
ScienceDirect
Ceramics International 37 (2011) 3765–3769
CERAMICS INTERNATIONAL
www.elsevier.com/locate/ceramint

Short communication

Properties of RF magnetron sputtered 0.95 ($Na_{0.5}Bi_{0.5}$) TiO_3–0.05 $BaTiO_3$ thin films

Ying-Hsun Lin [a], Ping-Shou Cheng [a], Chia-Ching Wu [b], Tai-Ping Sun [c], Jing-Jenn Lin [c], Cheng-Fu Yang [d,*]

[a] Department of Electronic Engineering National Kaoshiung University of Applied Sciences, Kaohsiung, Taiwan, ROC
[b] Department of Electronic Engineering, Kao Yuan University, Kaohsiung, Taiwan, ROC
[c] Department of Applied Materials and Optoelectronic Engineering, National Chi Nan University, Taiwan, ROC
[d] Department of Chemical and Materials Engineering, National University of Kaohsiung, Kaohsiung, Taiwan, ROC

Received 4 March 2011; received in revised form 26 April 2011; accepted 4 May 2011
Available online 12 June 2011

Abstract

0.95 ($Na_{0.5}Bi_{0.5}$)TiO_3–0.05 $BaTiO_3$ + 2 wt% Bi_2O_3 (NBT–BT3) ceramic was used as a target and NBT–BT3 thin films were deposited at room temperature by changing the RF power from 75 W to 150 W. The thickness of the NBT–BT3 thin films increased from 203 to 478 nm as the RF power increased from 75 W to 150 W. At 75 W RF power, the deposited NBT–BT3 thin films displayed defective surfaces, whereas at RF power ≧ 100 W, the NBT–BT3 thin films displayed smooth surfaces. The grain sizes also increased with increasing RF power. In addition, the remanent polarization and saturation polarization increased with increasing RF power. The coercive field first increased, reached a maximum at 100 W, then decreased with increasing RF power.

Keywords: A: Films; C: Electrical properties; D: Perovskites

1. Introduction

Nonvolatile ferroelectric random access memories have been proposed as next generation nonvolatile memory due to their excellent performance [1]. With the 1T1C (one transistor, one capacitance) structure, three different methods are used to increase the capacitance value of memory devices. The first method is to increase the electrode area of dielectric thin films; nevertheless, this method is not helpful because it brings an increase of the electrode area. The second method is to reduce the thickness of dielectric thin films, but this may lead to the electron tunneling effect. Thus, the ideal material would be one with a high dielectric constant and low leakage current density. Many ferroelectric thin-film materials are used as gate oxides, such as Pb(Zr,Ti)O_3 [2,3], $SrBi_2Ta_2O_9$ [4], $SrTiO_3$ [5], Ba(Zr,Ti)O_3 [6], and (Ba,Sr)TiO_3 [7]; these are being widely studied for larger storage capacity FeRAM devices because of their higher remanent polarization and lower coercive field.

Sodium bismuth titanate, $Na_{0.5}Bi_{0.5}TiO_3$ (NBT), is a kind of perovskite ABO_3-type ferroelectric material, discovered in 1960 [8]. NBT ceramic has been considered a strong candidate because of its marked ferroelectricity and piezoelectricity, excellent dielectric properties, and low loss tangent [9,10]. In spite of the numerous studies on NBT-based ceramics, investigations of the dielectric properties in NBT-based thin films are still in their infancy [11,12]. In this study, we investigated the composition of 0.95 ($Na_{0.5}Bi_{0.5}$)TiO_3–0.05 $BaTiO_3$ (NBT–BT3) thin films near the morphotropic phase boundary (MPB), deposited at different RF powers; the material features at the MPB usually have an extremely large dielectric constant [13,14]. During the fabrication of bismuth-based ferroelectric materials, excess Bi_2O_3 can be used to compensate for the vaporization of Bi_2O_3 and thereby improve ferroelectric properties and crystal structure [15]. Accordingly, in the present study 2 wt% excess Bi_2O_3 was added to the NBT–BT3 ceramic target to compensate for the vaporization of Bi_2O_3 during the deposition process. RF power was found to have large effects on the characteristics of NBT–BT3 thin films. The effects of RF power on the electrical characteristics of the deposited NBT–BT3 thin films, including polarization–applied

* Corresponding author.
E-mail address: cfyang@nuk.edu.tw (C.-F. Yang).

0272-8842/$36.00.
doi:10.1016/j.ceramint.2011.05.145

electrical field (*P–E*) and leakage current density–electrical field (*J–E*), are discussed in this study.

2. Experimental procedures

Na_2CO_3, Bi_2O_3, $BaCO_3$, and TiO_2, each with a purity of ≧99.5%, were used as starting materials. They were mixed to achieve 0.95 $(Na_{0.5}Bi_{0.5})TiO_3$–0.05 $BaTiO_3$ + 2 wt% Bi_2O_3 (NBT–BT3), and ball-milled for 5 h in deionized water. After being dried and ground, the NBT–BT3-*x* powders were calcined at 900 °C for 2 h, then ground again and mixed with polyvinylalcohol (PVA) as a binder. The powder was uniaxially pressed into pellets of 1 mm thickness and 12 mm diameter using a steel die. After debindering, the pressed target was sintered at 1200 °C for 2 h. The NBT–BT3 thin films were deposited at room temperature and a chamber pressure of 10 mTorr in pure argon by changing the RF power from 75 W to 150 W. They were then deposited onto SiO_2/p-Si(1 0 0)/Al and Pt/Ti/SiO_2/p-Si(1 0 0) substrates by RF magnetron sputtering for both the metal–ferroelectric–insulator–semiconductor (MFIS) and the metal–ferroelectric–metal (MFM) structures. The surface morphologies and thicknesses of the NBT–BT3 thin films were characterized by field emission scanning electron microscopy (FE-SEM), and their crystalline structures were identified by X-ray diffraction (XRD). To finish the MFM and MFIS structures, an array of circular top contacts with a diameter of 1 mm was formed by depositing Al thin films. The leakage current density-electrical field (*J–E*) characteristics were measured by a semiconductor parameter analyzer (HP 4156). The remanent polarization (Pr), saturation polarization (Ps), and coercive field (Ec) properties were measured by a Sawyer-Tower circuit (RT66A).

3. Results and discussion

As the RF power increases, more molecules are removed from the surface of the NBT–BT3 target and the deposition rate increases, so the thickness of the NBT–BT3 thin films increases with increasing RF power to 203, 256, 345, and 478 nm for RF powers of 75, 100, 125, and 150 W, respectively (Fig. 1).

The morphologies of the NBT–BT3 thin films deposited with various powers are shown in Fig. 2. The 75 W-deposited NBT–BT3 thin films exhibit a rugged and rough surface. When the RF is ≧100 W, the deposited NBT–BT3 thin films are smooth. Fig. 2 also shows the nano-crystalline structure of the NBT–BT3 grains, whose grain size increases with increased RF power, suggesting that the crystallization degree of the NBT–BT3 thin films increases with increasing RF power.

Fig. 3 shows the XRD patterns of NBT–BT3 thin films under different RF powers. At 75 W the amorphous phase and the (1 1 0) diffraction peak coexist, while at RF ≧ 100 W the amorphous phase decreases and even disappears, so only the crystalline NBT–BT3 phase may be detected and compared to standard JCPD cards. The crystalline peaks of all the NBT–BT3

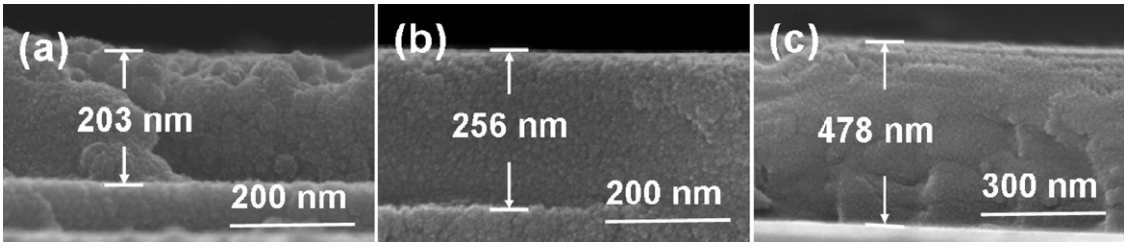

Fig. 1. Cross section of NBT–BT3 thin films under different RF powers (a) 75 W, (b)100 W, and (c)150 W.

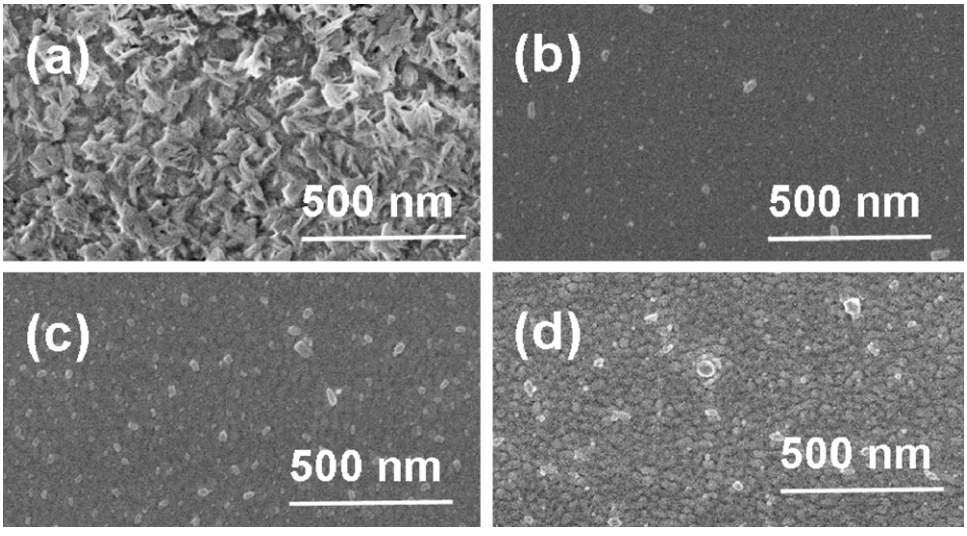

Fig. 2. Surface observations of NBT–BT3 thin films as a function of deposition power (a) 75 W, (b) 100 W, (c) 125 W, and (d) 150 W.

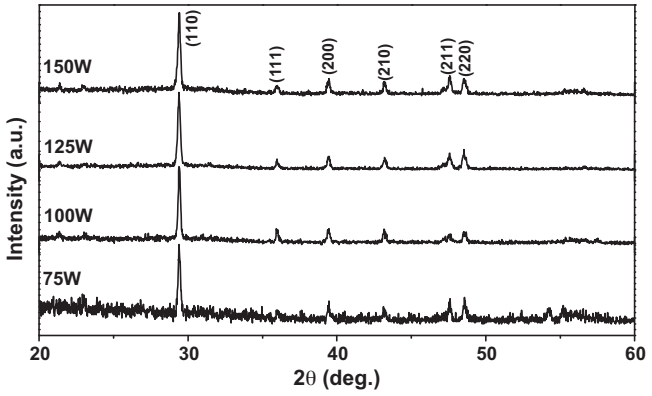

Fig. 3. X-ray diffraction patterns of NBT–BT3 thin films as a function of deposition power.

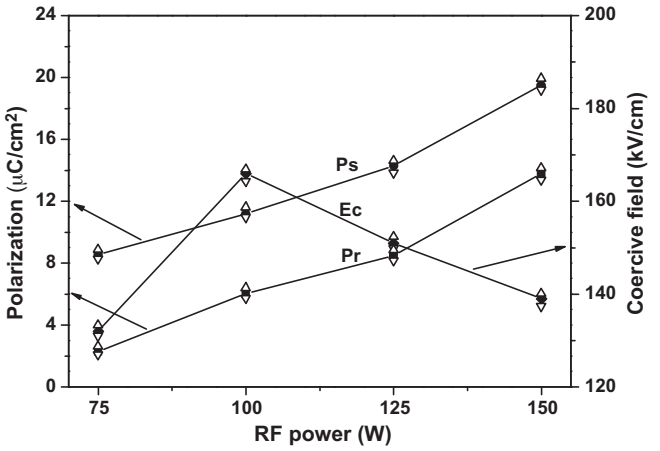

Fig. 5. The Pr, Ps, and Ec of NBT–BT3 thin films as a function of depositing power.

thin films are shifted to lower 2θ values due to residual titanium in the thin films, which affects the lattice constants, as reported by Wang et al. [16].

The ferroelectric properties of the MFM structure of the NBT–BT3 thin films were investigated using the Sawyer-Tower circuit. The Pr, Ps, and Ec values are calculated from the hysteresis loops of the NBT–BT3 films shown in Fig. 4. Results in Fig. 5 indicate that the RF power affects the Pr, Ps, and Ec values. For 75 W-deposited NBT–BT3 thin films, the Pr, Ps, and Ec values are 2.30 μC/cm^2, 8.56 μC/cm^2, and 132 kV/cm. As the RF power increases, the Pr and Ps values increase and the Ec value initially increases, reaching a maximum when the RF power is 100 W. In Fig. 2, the surface SEM micrographs for the NBT–BT3 thin films deposited at 75 W show a rugged and rough structure. At an RF power of 100 W, the roughness is lessened and particle crystallization is observable. The Pr, Ps, and Ec values are dominated by grain size growth and the crystallization of the NBT–BT3 thin films. As the RF power is equal to and then greater than 100 W, the increase in the grain growth is the reason for the increases in the Pr and Ps values and the decrease in the Ec value. Thus, NBT–BT3 thin films deposited under 150 W have maximum Pr and Ps values of 13.8 μC/cm^2 and 19.5 μC/cm^2 and a minimum Ec value of 139 kV/cm.

The leakage current behaviors of the NBT–BT3 thin films were investigated to determine the leakage current density (J) and electrical field (E) characteristics and the results are shown in Fig. 6. The leakage current density of the MFIS thin films plays an important role in alleviating the interdiffusion between silicon and the NBT–BT3 thin films under the different deposition parameters. Using 75 W and 100 W as the RF power, the leakage current densities of the NBT–BT3 thin films increases from 1×10^{-10} A/cm^2 to 1×10^{-7} A/cm^2 and 3×10^{-8} A/cm^2 as the electrical field increases from 0 MV/cm to 2 MV/cm. When 125 W and 150 W are used as the RF power, the electrical field increases from 0 MV/cm to 2 MV/cm and the leakage current densities are less than 1×10^{-8} A/cm^2. It is believed that as the RF power increases, the decreased roughness and increased thickness produce those results.

The linear variations of leakage current densities correspond either to the Schottky emission mechanism or to the Poole-Frenkel emission mechanism. The current density (J) in the Schottky emission mechanism is generated by the thermionic effect, which is caused by electron transport across the potential

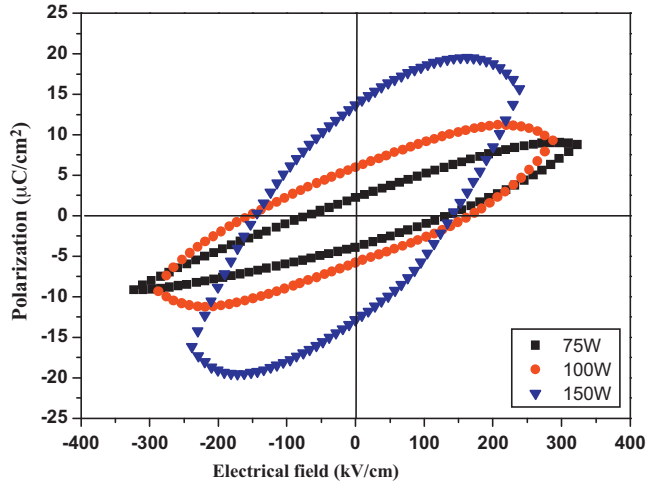

Fig. 4. P–E curves of NBT–BT3 thin films as a function of deposition power.

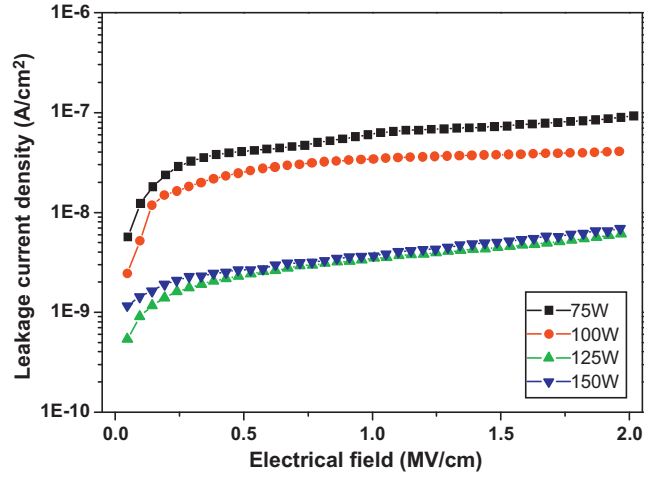

Fig. 6. J–E curves of NBT–BT3 thin films as a function of deposition power.

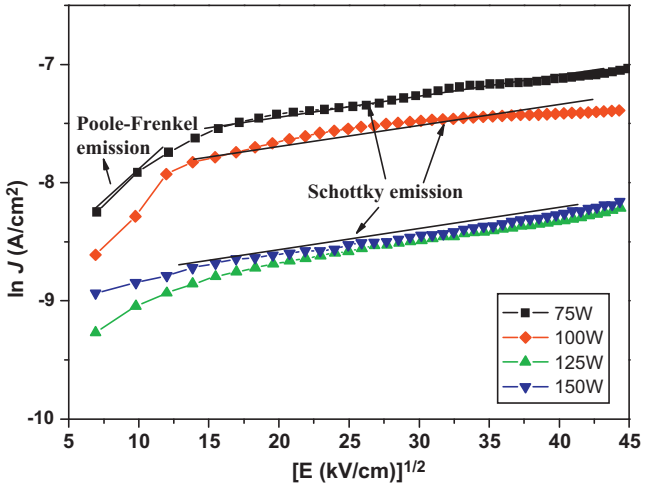

Fig. 7. log J–$E^{1/2}$ plots of NBT–BT3 thin films.

energy barrier via field-assisted lowering at a metal–insulator interface, as given by Eq. (1) [17]:

$$\alpha = \left[\frac{B(h\upsilon - E_g)^p}{h\upsilon}\right] \quad (1)$$

where $\beta_s = (e^3/4\pi\varepsilon_o\varepsilon)^{1/2}$ and e is the electron charge, ε_o is the dielectric constant of free space, and A^* is the effective Richardson constant. The current density (J) in the Poole-Frenkel emission mechanism is due to field-enhanced thermal excitation of trapped electrons from the insulator into the conduction band, as given by Eq. (2) [18]:

$$\alpha\left[\frac{1}{d}\ln\left(\frac{1}{T}\right)\right] \quad (2)$$

where $J_o = \sigma_o E$ is the low-field current density, $\beta_{PF} = (e^3/\pi\varepsilon_o\varepsilon)^{1/2}$, σ_o is the low-field conductivity, ψ_{PF} is the height of the trap potential well, and T is the absolute temperature. Fig. 7 shows the J–E characteristics with ln(J) as the vertical axis and $E^{1/2}$ as the horizontal axis. From the ln J–$E^{1/2}$ curves of the NBT–BT3 thin films shown in Fig. 7, it can be determined that the leakage current density is linearly related to the square root of the applied electric field.

The experimental results in Fig. 7 indicate that the 75 W- and 100 W-deposited NBT–BT3 thin films exhibit the Poole-Frenkel emission mechanism under the low electric field of 0∼140 kV/cm ($E^{1/2}$ = 0–12 (kV/cm)$^{1/2}$). This means that the carriers are transported through the NBT–BT3 thin films by the field-enhanced Poole-Frenkel emission mechanism in the low electrical field region. Fig. 7 also shows 75 W- and 100 W-deposited NBT–BT3 thin films exhibiting the Schottky emission mechanism, as the electrical field is >230 kV/cm ($E^{1/2}$ > 15 (kV/cm)$^{1/2}$). For the 125 W- and 150 W-deposited NBT–BT3 thin films, the ln J–$E^{1/2}$ curves are dominated by the Schottky emission mechanism. Comparing the different curves in Fig. 7 shows that the all NBT–BT3 thin films in the high electrical field region have the same slopes. These results also prove that the ln J–$E^{1/2}$ curves are dominated by the Schottky emission mechanism, and the leakage current densities of the NBT–BT3 thin films are mainly caused by electron transport across the potential energy barrier. The decrease in leakage current density with increasing RF power occurs because as the RF power increases the defects on the surfaces of the NBT–BT3 thin films decrease.

4. Conclusions

The influences of RF power on the characteristics of NBT–BT3 thin films were explored. For the as-deposited NBT–BT3 thin films, the grain sizes increased with increasing RF power. In the leakage current density versus electrical field (J–E) curves, the leakage current density decreased with increasing RF power, reaching a saturation value when the RF power was 125 W. As the RF power increased, the Pr and Ps values increased and the Ec value increased to a maximum when the RF power was 100 W. The NBT–BT3 thin films deposited under 150 W had maximum Pr and Ps values of 13.8 μC/cm^2 and 19.5 μC/cm^2 and the minimum Ec value was 139 kV/cm. Thus, it was demonstrated that RF power plays an important role in affecting the characteristics of NBT–BT3 thin films.

Acknowledgements

The authors will acknowledge to the help of Mr. Lin-Yu Wong in experimental process and financial support of NSC 99-2221-E-390-013-MY2.

References

[1] H. Buhay, S. Sinharoy, W.H. Kasner, M.H. Francombe, D.R. Lampe, E. Stepke, Pulsed laser deposition and ferroelectric characterization of bismuth titanate films, Applied Physics Letters 58 (1991) 1470–1472.
[2] H.H. Park, R.H. Hill, Stacking effect on the ferroelectric properties of PZT/PLZT multilayer thin films formed by photochemical metal-organic deposition, Applied Surface Science 237 (2004) 427–432.
[3] S.W. Bae, H.H. Park, T.S. Kim, Ferroelectric properties of direct-patterned half-micron thick PZT film, Sensors and Actuators A: Physical 125 (2006) 548–552.
[4] M. Moert, T. Mikolajick, G. Schindler, N. Nagel, I. Kasko, W. Hartner, C. Dehm, H. Kohlstedt, R. Waser, Integration of stacked capacitor module with ultra-thin ferroelectric $SrBi_2Ta_2O_9$ film for high density ferroelectric random access memory applications at low voltage operation, Thin Solid Films 473 (2005) 328–334.
[5] C.S. Hwang, S.O. Park, C.S. Kang, H.J. Cho, H.K. Kang, S.T. Ahn, M.Y. Lee, Deposition and electrical characterization of very thin $SrTiO_3$ films for ultra large scale integrated dynamic random access memory application, Japanese Journal of Applied Physics 34 (1995) 5178–5183.
[6] C.F. Yang, K.H. Chen, Y.C. Chen, T.C. Chang, Fabrication of one-transistor-capacitor structure of nonvolatile TFT ferroelectric RAM devices using $Ba(Zr_{0.1}Ti_{0.9})O_3$ gated oxide film, IEEE Transactions on Ultrasonics Ferroelectrics, and Frequency Control 54 (2007) 1726–1730.
[7] P. Mounaix, M. Tondusson, L. Sarger, D. Michau, V.R.M. Maglione, High-frequency response in ferroelectric $BaSrTiO_3$ thin films studied by terahertz time-domain spectroscopy, Japanese Journal of Applied Physics 44 (2005) 5058–5061.
[8] G.A. Smolenskii, V.A. Isupov, A.I. Agranovskaya, N.N. Krainik, New ferroelectrics of complex composition, Physics of the Solid State 2 (1961) 2651–2654.
[9] N. Scarisoreanu, F. Craciun, V. Ion, S. Birjega, M. Dinescu, Structural and electrical characterization of lead-free ferroelectric $Na_1/2Bi_1/2TiO_3$–

$BaTiO_3$ thin films obtained by PLD and RF-PLD, Applied Surface Science 254 (2007) 1292–1297.

[10] T. Kimura, T. Takahashi, T. Tani, Y. Saito, Preparation of crystallographically textured $Bi_{0.5}Na_{0.5}TiO_3$–$BaTiO_3$ ceramics by reactive-templated grain growth method, Ceramic International 30 (2004) 1161–1167.

[11] D.Y. Wang, D.M. Lin, K.S. Wong, K.W. Kwok, J.Y. Dai, H.L.W. Chan, Piezoresponse and ferroelectric properties of lead-free $[Bi_{0.5}(Na_{0.7}K_{0.2}Li_{0.1})_{0.5}]TiO_3$ thin films by pulsed laser deposition, Applied Physics Letters 92 (2008) 222909–222912.

[12] D. Alonso-Sanjosé, R. Jimenez, I. Bretos, M.L. Calzada, Lead-free ferroelectric $(Na_{1/2}Bi_{1/2})TiO_3$–$BaTiO_3$ thin films in the morphotropic phase boundary composition: solution processing and properties, Journal of the American Ceramic Society 92 (2009) 2218–2225.

[13] J. Rouquette, J. Haines, V. Bornand, M. Pintard, Ph. Papet, C. Bousquet, L. Konczewicz, F.A. Gorelli, S. Hull, Pressure tuning of the morphotropic phase boundary in piezoelectric lead zirconate titanate, Physical Review B 70 (2004) 014108–014112.

[14] Y. Li, W. Chenb, Q. Xub, J. Zhoub, X. Gua, S. Fang, Electromechanical and dielectric properties of $Na_{0.5}Bi_{0.5}TiO_3$–$K_{0.5}Bi_{0.5}TiO_3$–$BaTiO_3$, Materials Chemistry and Physics 94 (2005) 328–332.

[15] Y.F. Wei, C.F. Yang, C.Y. Chen, C.J. Huang, C.H. Kao, Development of non-stoichiometric $SrBi_{4+2x}Ti_4O_{15+3x}$ $(-0.04 \leq x \leq 0.04)$ ceramics, advances in applied ceramics: structural, Functional and Bioceramics 108 (2009) 102–105.

[16] X.X. Wang, S.W. Or, X.G. Tang, H.L.W. Chan, P.K. Choy, P.C.K. Liu, TiO_2-nonstoichiometry dependence on piezoelectric properties and depolarization temperature of $(Bi_{0.5}Na_{0.5})_{0.94}Ba_{0.06}TiO_3$ lead-free ceramics, Solid State Communications 134 (2005) 659–698.

[17] P. Hesto, G. Barvotlin, A. Vapaille, Instabilities in Silicon Devices, North-Holland, Amsterdam, 1986.

[18] S.M. Sze, Physics of Semiconductor Devices, Wiley, New York, 1981.